RESEARCH ARTICLE

The effect of acid/cellulose ratio on the quality of Cellulose Nanocrystal (CNC) suspension

Nasrin Shahmiri[1], Nahid Hassanzadeh Nemati[1]*, Ahmad Ramazani Saadatabadi[2], Massoud Seifi[3]

[1] Department of Biomedical Engineering, Science and Research Branch, Islamic Azad University, Tehran, Iran.

[2] Department of Chemical & Petroleum Engineering, Sharif University of Technology, Tehran, Iran.

[3] Department of Orthodontics, School of Dentistry, Shahid Beheshti University of Medical Sciences, Tehran, Iran.

ARTICLE INFO

Article History:
Received 2022-04-10
Accepted 2022-07-24
Published 2022-12-22

Keywords:
Cellulose Nanocrystal, Synthesis, Filter paper, Acid hydrolysis, Acid-to-cellulose ratio, Acid-to-pulp ratio, Acid-to-paper ratio, Zeta-potential, Particle size, Dynamic Light Scattering, Atomic Force Microscopy

ABSTRACT

Cellulose nanocrystals are promising materials for application in the biomedicine, pharmaceutical, and food industries. There are various methods for CNC synthesis, but acid hydrolysis is the most common one. The optimization of the acid hydrolysis process is still in progress. In the present study, different CNC suspensions were prepared to find out the more efficient acid ratio for CNC production. Whatman #1 filter paper was hydrolyzed via 64 wt% sulfuric acid at an acid-to-paper ratio of 10:1 mL/g, 20:1 mL/g, 30:1 mL/g, and 40:1 mL/g. The synthesized CNCs were characterized by DLS, ELS, and AFM. The suspensions with acid-cellulose ratio of 20:1 mL/g & 30:1 mL/g resulted in CNCs with more negative surface charge and uniform size. The CNCs showed chiral nematic phase and regular self-organization after layer-by-layer deposition. It was found that the higher acid-to-paper ratio does not necessarily produce high-quality CNCs. The size and surface charge of CNCs are highly dependent on acid hydrolysis parameters that affect their behavior in nano-composites. Despite many published papers around CNC synthesis by acid hydrolysis, there are still some details that must be investigated more to prepare the most efficient and applicable CNCs.

How to cite this article
Shahmiri N., Hassanzadeh Nemati N., Ramazani Saadatabadi A., Seifi M., The effect of acid/cellulose ratio on the quality of Cellulose Nanocrystal (CNC) suspension. J. Nanoanalysis., 2022; 9(4): 294-311. DOI: 10.22034/jna.2022.1946948.1270

INTRODUCTION

Cellulose and its derivatives are widely used for developing and constructing smart organic/inorganic hybrid materials (1). Cellulose nanocrystals (CNCs) are one of the fantastic derivatives of cellulose. They have outstanding properties, such as inherent renewability, biodegradability, flexibility, printability, low density, high elastic modulus, high porosity, dimensional stability, and optical transparency. CNC has been successfully conjugated with other nanomaterials, yielding new nanohybrid materials with different applications, including materials science, electronics, and medicine (2-5). Several nanomaterials can be utilized for the degradation of pollutants from aqueous environments (6-12). In this regard, the application of CNCs in the bioremediation field is promising, both in metal sorption from wastewater or as an alternative for water desalination (13). CNC colloidal suspension can also be used in various biotechnological and biomedical fields (14). Thus, researchers are still working on the efficient obtainment and smart application of CNCs (4).

The dimensions of CNCs vary in the literature. They are in the range of 5–50 nm in diameter and 100–500 nm in length (15). The basic principle of

* Corresponding Author Email: *nahid_hasanzadeh@yahoo.com*

nanocrystalline cellulose synthesis is the isolation of the amorphous regions in the cellulose fiber structures (16). Acid hydrolysis is one of the most common methods of CNC production. During acid hydrolysis, the β-1,4 glycosidic bond is broken, which will shorten the polymer chains and decrease the physical dimensions (17). Nascimentoa et al. (18) showed that the acidic route is an efficient method for obtaining monodisperse cellulose nanowhiskers from industrial cotton wastes. Acid hydrolysis results in CNCs with a higher crystallinity index and better size dispersion (19).

Sulfuric acid (H_2SO_4) is a suitable acid to generate stable, homogeneous, and re-dispersible CNCs due to the electrostatic repulsive interaction of negatively charged sulfate groups with hydroxyl groups of CNCs (16, 20). Lu & Hsieh (21) utilized sulfuric acid to remove amorphous cellulose and produce isolated cellulose nanocrystals with newly introduced sulfate groups on the nanocrystal surfaces. So the surface of CNCs is expected to be full of hydroxyl groups of cellulose and negatively charged sulfate half-ester groups after sulfuric acid hydrolysis (22). The strong acid sulfate half-ester groups diminish the negative zeta-potential and improve the colloidal stability of aqueous CNC suspension (15, 22). Indeed, sulfuric acid extracted CNCs are material with comparable particle dimensions and properties (23).

The efficiency of hydrolysis reaction can be promoted by changing the hydrolysis conditions, including the acid type, acid concentration, acid/cellulose ratio, temperature, as well as reaction time, and these factors influence the shapes, sizes, and properties of isolated CNCs (15, 16). Moreover, the uniform dispersion of CNCs in a polymer matrix is a big challenge, since aggregation or agglomeration often occurs (2).

Surface charge density, crystallinity, and particle dimensions can affect CNC behavior. There are abundant hydroxyl groups on the surface of CNCs that can be used for functionalization (24). The self-assembly and formation of chiral nematic phases in CNC suspensions are indicators of good particle behavior. The CNC properties must be evaluated through complete characterization (23). However, DLS and AFM are among the most important prerequisites. DLS (Dynamic Light Scattering) presents the hydrodynamic "apparent particle size" of cellulose nanocrystal suspensions. Zeta potential shows surface potential and colloidal stability (23). The determination of zeta potential is valuable for controlling the stability of a colloidal system (25). DLS technique is very helpful to better clarify the role of the colloidal interactions (26). The atomic force microscope (AFM) is also an important imaging tool to prove successful CNC synthesis. It can provide us CNC images with good contrast and relatively low cost. The shape and dimensions of CNCs are determined by AFM. The atomic force microscope measures interaction forces between the sample and a tip attached to a cantilever as the tip is raster scanned across the surface (27). Thus, DLS and AFM together can provide primary useful information about the size and shape of CNCs.

The shape and size of the CNCs are dependent on the source material as well as the synthesis conditions (28). There are numerous descriptions of the acid hydrolysis process for CNC synthesis in the literature. Some studies utilized an acid-to-cellulosic material ratio of 10:1 mL/g and the others utilized 20:1 mL/g. For example, Lu et al. (21) & Feng et al. (29) hydrolyzed filter paper at the acid-to-paper ratio of 10:1 mL/g by 64 wt% sulfuric acid. Hamad (30) suggested an acid-to-pulp ratio of 6 - 8.75:1 mL/g by 64 wt% sulfuric acid to produce CNCs. Santana et al. (31) hydrolyzed cotton linter by 65 wt% sulfuric acid at an acid-to-cotton ratio of 20:1 mL/g. Mascheroni et al. (32) utilized an acid-to-fiber ratio of 17.5:1 mL/ g for hydrolyzing cotton linters by 64 wt% sulfuric acid. Gray et al. (33) also hydrolyzed Whatman cotton powder with 64 wt% sulfuric acid at an acid/cellulose ratio of 17.5:1 mL/g.

Despite the numerous published papers around CNCs, there are still points that need to be explored further. The effect of the acid-to-cellulose ratio has not been completely investigated in the literature. Moreover, it is well-known that changes to cellulose source and hydrolysis conditions can drastically impact CNC properties and behavior (23). So, this study was done based on the question "What is the more efficient acid-to-paper ratio for CNC extraction, especially from filter paper?". Then, different CNC suspensions were prepared and characterized to evaluate the size, surface charge, and shape of the produced CNCs via DLS, ELS, and AFM, respectively.

MATERIALS & METHODS:

Materials:

Whatman #1 filter paper (Qualitative, 7cm, England), Whatman #541 hardened ashless filter paper (9 cm, pore size 22 μm, England), Sulfuric

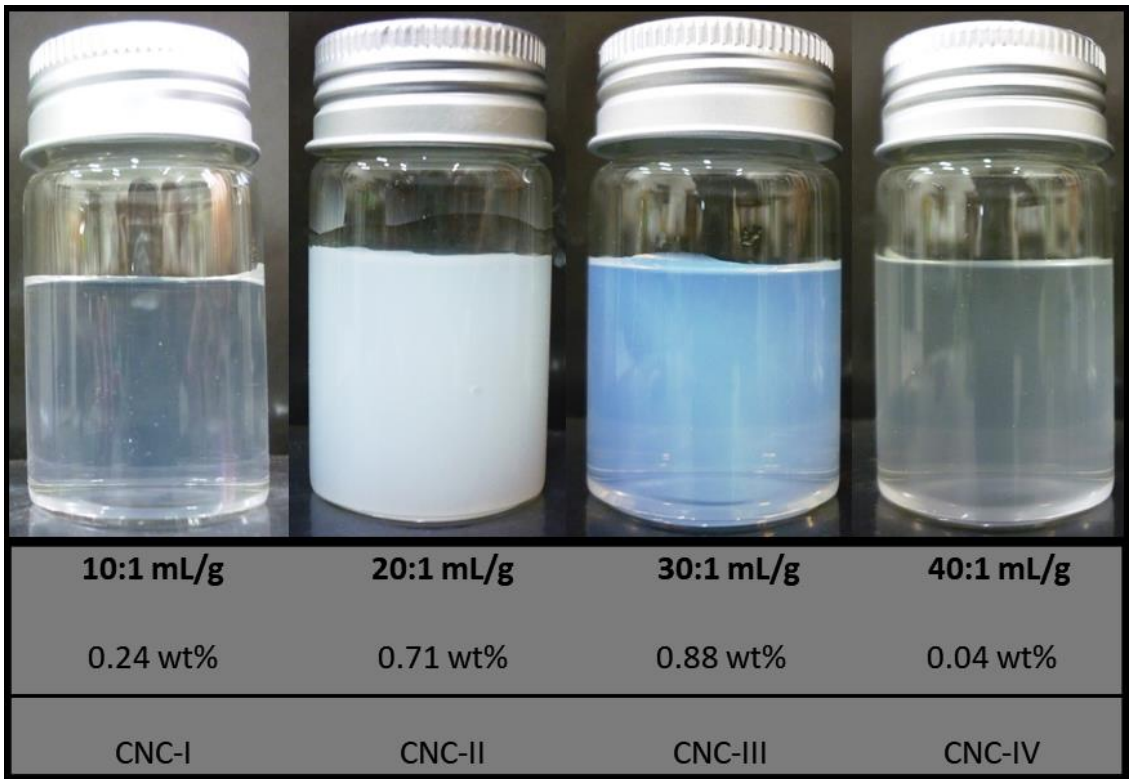

Fig. 1. The final synthesized CNC slurries with corresponding acid-to-paper ratio and concentration.

acid (H_2SO_4 95-97%, Merck, Germany), Dialysis tubing membrane (43 mm, MWCO 12-14 kDa, Sigma-Aldrich, Germany), Acetone (CH_3COCH_3 99.5% purity, Asiapajohesh Co, Iran), Ethyl Alcohol (C_2H_5OH 96% v/v, Nasr Alcohol Co, Iran), Hydrogen peroxide (H_2O_2 3%, Kimiagartoos Co, Iran), Double distilled water (ddH_2O, Nabet Co, Iran), Microscope cover glass (18×18 mm, 0.13-0.17 mm thickness, Sail Brand, China). (All chemicals were used without further purification)

CNC synthesis:

The process of CNC synthesis was designed based on previous studies (16, 20, 21, 29, 34-40). The Whatman #1 filter paper (2.5 gr) was ground, and hydrolyzed by sulfuric acid (64 wt%) at 45 °C for 60 min by gentle mechanical stirring. Four samples were prepared at an acid-to-paper ratio of 10:1 mL/g, 20:1 mL/g, 30:1 mL/g, and 40:1 mL/g and named CNC-I, CNC-II, CNC-III, and CNC-IV, respectively (2.5 gr filter paper for each sample). The hydrolysis reaction was quenched with 10-fold chilled ddH_2O (3 °C). The solutions were allowed to settle for 3 days. After that, the clear supernatants were decanted and the resultant white slurries were centrifuged at 4100 rpm for 30 minutes. The clear supernatants were discarded again and the thick white pellet redispersed in ddH_2O by mechanical agitation. The resulting CNCs were dialyzed against ddH_2O until the pH of dialysate remained constant and conductivity remained below 5 µS/cm. Then CNC suspensions were undergone probe sonication for 10 min at 60% amplitude with a 9.5 mm diameter tip, continuously. After that CNC suspensions were filtered via Whatman #541 ashless filter paper. Finally, they were stored at + 4 °C for later characterization. The appearance and concentration of final suspensions can be seen in Fig. 1. All photographs were taken by a digital camera.

Characterization:

Dynamic Light Scattering (DLS):

The particle size distribution and zeta-potentials were determined by dynamic light scattering (DLS) and electrophoretic light scattering (ELS), respectively. Particle Size and Zeta Potential Analyzer (Brookhaven Instruments, NanoBrook, 90Plus Zeta Particle Size Analyzer, USA), was utilized at a detection

angle of 90° for size measurement, 15° for zeta-potential determination, and wavelength of 640 nm. A 35-mW red diode laser was utilized as the light source. The NanoBrook 90Plus has a sizing range of > 1 nm to 6 μm diameter in a concentration range of 2 ppm to 50 mg/mL for DLS and a size range of 1 nm to 100 μm in a concentration range of 40% v/v, for ELS. Mobility values are converted to zeta-potentials using the Smoluchowski equation. All four suspensions were probe-sonicated for 10 min at 60% amplitude with a 9.5 mm diameter tip (Ivymen, CY-500, Homogeneizador, Spain) continuously, before DLS and ELS to obtain a homogeneous suspension before the measurement. Measurements were performed in ambient conditions. Around 2 ml of sample was placed in a cuvette and placed in the instrument for DLS analysis. The apparatus performed measurements of samples in triplicate for DLS and 30 times for ELS and measurements were averaged together. The suspensions were analyzed with two different concentrations for a better conclusion. First, the original primary suspensions with corresponding concentrations (Fig. 1) were analyzed by DLS and ELS, and then the diluted suspensions (0.025 wt%) were analyzed according to previous studies (23, 41).

Atomic Force Microscopy (AFM):

Atomic Force Microscopy (AFM) was carried out by using a Nanosurf Easyscan C3000 (Firmware version 3.5.0.29, Software version 3.5.0.29, Switzerland). AFM tip radius was 10 nm. Four images were obtained at a resolution of 256×256 pixels from each sample. The vibration frequency was 139.386 kHz. The vibration amplitude, excitation amplitude, cantilever type, head type, and setpoint were 250 mV, 666 mV, Tap190AI-G, FlexAFM, and 50%, respectively. Imaging was performed with non-contact and phase contrast mode at room temperature in the air. Scans of 10×10 μm^2 and 5×5 μm^2 were performed to analyze the shape of CNCs. CNC suspensions were adjusted to 0.001 wt%, sonicated for 10 min at 60% amplitude (continuous, 9.5 mm diameter tip), then dropped (0.3 ml) onto a microscope cover glass and allowed to dry in the air for 4 hours. Moreover, 3 drops (0.3 mL/drop) of original primary suspensions without further dilution were deposited on microscope cover glass with layer by layer technique. The first drop was deposited on the substrate and after drying the second drop was deposited and allowed to dry. At last, the third drop was deposited with the same procedure. This process was done to make a comparison regarding morphology between concentrated and diluted CNCs. The CNC films were placed in a polystyrene Petri dish before the AFM test, as there was a gap between film preparation and AFM analysis. The main goal of AFM characterization was only to prove the production of CNCs by their rod-shaped or needle shape.

RESULTS & DISCUSSIONS:

CNCs were extracted from Whatman #1 filter paper (cotton cellulose) by sulfuric acid hydrolysis. The acid cleaves the glucosidic linkages in the amorphous region of cellulose and leaves the CNCs. Fig. 1 shows the final CNC suspensions. Here, produced CNCs were characterized by DLS, ELS, and AFM. The dynamic light scattering was used to determine the size distribution of CNCs. This method measures the translational diffusion of the particles in the suspension (42). AFM can also be utilized for the size measurement of CNCs, but it was done only to prove the presence of cellulose nanocrystals and show their shape as needle-like or rod-like. In fact, the size analysis via AFM is so time-consuming (43). It needs at least 100 individual CNCs in AFM images to report a reliable estimation of CNC dimensions. DLS can provide rapid evaluation of particle size (43). The colloidal stability of produced CNCs was assessed by ELS and zeta potentials.

DLS-ELS: Original CNC suspensions

The average hydrodynamic diameters of CNCs are summarized by details in Table 1. The CNCs' diameters by intensity are consistent with previous studies (31, 32, 41, 44, 45). The apparent diameter of CNC-II and CNC-III are lower than CNC-I and CNC-IV. The CNC-III suspension had the smallest particles (Table 1). The diameters of particles in CNC-I and IV suspensions were 484.56 ± 66.10 nm and 465.82 ± 149.64 nm, respectively. Vanderfleet et al. (41) did not consider CNCs with large particle sizes around 351 ± 6 as true CNCs, partly because of the large size and partly because of the brown color observed after hydrolysis. It seems that harsh acid hydrolysis conditions beyond a certain point can damage the crystalline region. The brown color of the hydrolysis mixture might be due to the furfural and 5-hydroxymethyl-2-furfural (HMF), which are degradation products

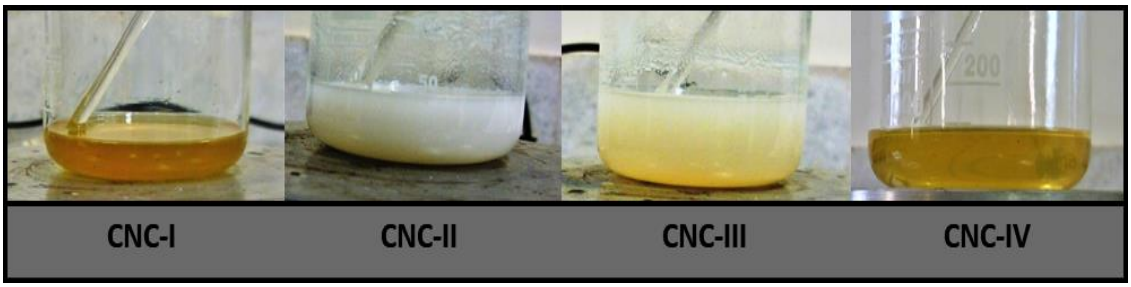

Fig. 2. The appearance of hydrolysis mixtures.

Table 1. The average zeta-potential, pH, mean polydispersity and diameters of original CNC suspensions.

Sample	Zeta potential (mV)	pH of suspensions	Polydispersity Index	Diameter By Intensity (nm)	Diameter By Number (nm)	Diameter By Volume (nm)
CNC-I	− 20.64	5	0.3 ± 0.04	484.56 ± 66.10	43.78 ± 20.53	226.19 ± 87.47
CNC-II	− 28.58	5	0.2 ± 0.01	255.02 ± 18.08	27.72 ± 25.78	80.50 ± 72.70
CNC-III	− 32.24	6	0.3 ± 0.01	115.41 ± 6.99	7.77 ± 2.41	9.06 ± 2.69
CNC-IV	− 24.11	6	0.2 ± 0.04	465.82 ± 149.64	235.26 ± 139.74	569.25 ± 272.99

from the hydrolysis of CNCs (41). So, the yellow to brown color of the CNC-IV mixture during hydrolysis can be due to the huge amount of acid (Fig. 2). However, the color of the CNC-I hydrolysis mixture was brown, despite the lower acid volume. Moreover, the apparent diameter of CNC-I was larger than CNC-IV (Table 1). The mechanical stirring rate of the hydrolysis mixture was not constant in this research, as stirring was done manually with a glass rod. Despite our effort to preserve the other hydrolysis conditions (acid concentration, time, temperature) constant for all four samples, it would be possible that the stirring rate of the CNC-I mixture was more vigorous than three other samples leading to the brown color of CNC- I mixture.

There was a reasonable decrease in particle size as the acid-to-paper ratio was increased, and it can be seen that CNC-III has the smallest particle size. But the size of CNCs increased again by changing the acid-to-paper ratio from 30:1 mL/g to 40:1 mL/g (Table 1). Although the average intensity-based diameters obtained for CNC-I and CNC-IV are large numbers, the diameters by number and volume are smaller for CNC-I. Moreover, the diameter by number is smaller for CNC-IV, too. So, it is almost evident that the intensity-based diameters were overestimated mostly due to agglomeration that can't be distinguished by DLS. The DLS analysis will overestimate particle dimensions because it cannot differentiate between aggregates and single particles (17).

The intensity-based results of DLS can be affected by larger clusters (46). Because large agglomerates might dominate the obtained signal and mask the presence of smaller CNCs (13). Thus, size distribution by number and corresponding mean values were presented in Fig. 3 and Table 1, respectively. Size graphs by number are narrow with only one peak (Fig. 3). They help to understand better the CNCs' size and subpopulations. Therefore, it would be possible to make a reasonable comparison between suspensions. Fig. 3 shows that CNC-III had better homogeneity as three measurement peaks are rather overlapped which indicates more reliability (47). Three distribution graphs of CNC-III are sharper and narrower, too. On the other hand, multiple peaks can be seen in the graph of CNC-IV, partly due to agglomerations and partly due to its lowest concentration (Fig. 1). Because dilution of the sample affects the DLS size distribution graph based on Zhou et al.'s (48) study.

The measured zeta-potentials (Table 1) are consistent with previous studies (13, 18, 20, 42, 49), which show the presence of negatively charged CNCs in the final aqueous suspensions. The Zeta potential (ζ) is derived from the measurement of the particle mobility distribution when applied to an electric field (electrophoretic mobility) and is used to examine the stability of the nanocellulose

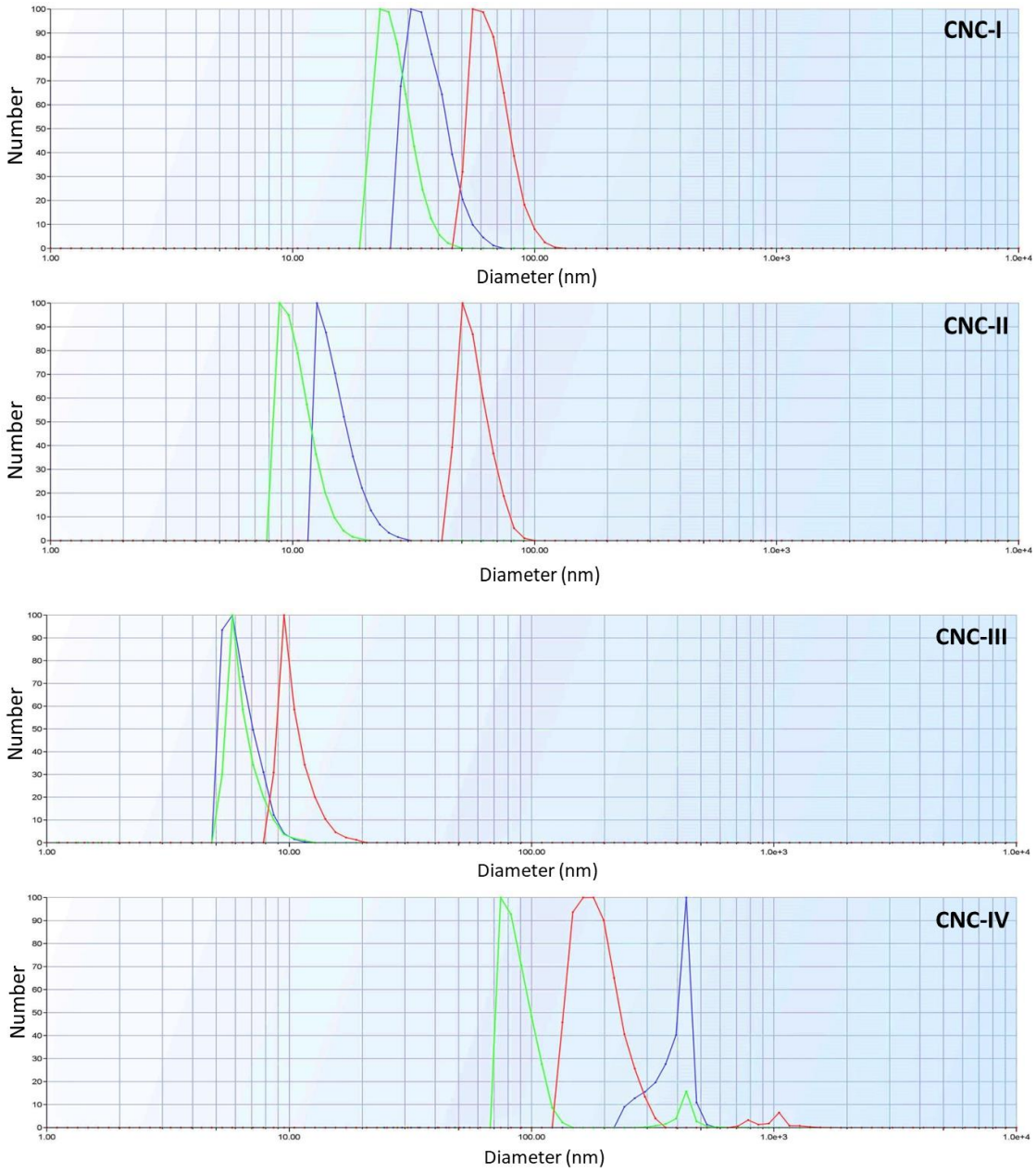

Fig. 3. The size distribution of original CNC suspensions obtained from DLS. (Red: first run, Green: second run, Blue: third run)

suspension in water (23, 42). The magnitude of the zeta-potentials in the present study shows the stability of the CNC suspensions due to the electrostatic repulsion between the sulfate groups on the surface of CNC rods (45). Although, nanoparticle dispersions with zeta potential value of ± 20–30 mV are classified as moderately stable dispersions (50). The CNC aqueous suspensions were homogenous and there was not any observable precipitation (Fig. 1). This is mainly due to the electrostatic interactions of CNCs in colloidal dispersion (51).

The CNC-III had the highest absolute zeta-potential value (32.24), which means the more negative surface charge (Table 1). So, it can be considered electrostatically stable due to the absolute value of zeta potential higher than 25mV (42). In fact, sulfate groups on the surface of CNCs induce electrostatic repulsive forces between nanocrystals, making the CNCs colloidal

suspension more stable over an extended time (52, 53).

It seems that, as the acid-to-paper ratio increased, there was a kind of logical increase in the absolute value of zeta-potential from CNC-I to CNC-III, regardless of CNC-IV (Table1). This result shows that a higher acid-to-paper ratio can induce more hydroxyl groups on the surface of CNC, resulting in more sulfate ester groups (54). The increased sulfate ester groups have a remarkable negative zeta-potential (51, 55). However, at a critical point, the zeta-potential absolute value decreased again (CNC-IV) (Table 1).

The final pH of CNC aqueous suspensions is consistent with previous studies (23, 56) (Table1). As the pH increased, the zeta-potential value decreased and became more negative in agreement with previous works (13) (Table 1). In other words, at higher pH, the absolute value of zeta potential increased which means that the electrical potential at the surface of the charged particle also increased; so the electrostatic repulsion forces between the charged particles become higher than the Van der Waals attractive forces, and the colloidal system will become stable (25). It is also worth mentioning that cellulose nanocrystals carry carboxylic acid groups, which undergo deprotonation at higher pH leading to negatively charged surfaces. As a result, the zeta-potential decreases with increasing pH (Table 1) (57) and becomes more negative, or in other words the absolute value of zeta-potential increases. Furthermore, cellulose nanocrystals, with their greater number of deprotonated carboxyl groups can improve the dispersive property in nanocomposites (57). The basis of the zeta-potential measurement is the Einstein–Smoluchowski electrical mobility equation. Accordingly, the results obtained are not absolute values, indeed DLS cannot accurately estimate the particles in the suspension, but the qualitative numeric results can be obtained quickly and can be used to compare samples qualitatively (49, 58). Zeta potential (estimated as surface charge) can be calculated by tracking the moving rate of negatively or positively spherical charged particles across an electric field (19). It is important to note that when calculating the zeta potential using the Smoluchowski or Hückel equation that assumptions are made about particle shape and behavior in an electric field. It would be more accurate to report electrophoretic mobility, yet zeta potential is usually presented in the literature (23). The electrophoretic mobility of CNC-I to CNC-IV was - 1.61, - 2.23, - 2.52, -1.88 (μ/s) (V/cm), respectively, which proves the higher mobility of CNC-II and CNC-III. It must be mentioned that electrophoretic mobility, and ultimately zeta potential, is influenced not only by sulfate ester content but particle shape and surface morphology (23). Although, sulfate half ester content is an important factor in CNC behavior and determines the colloidal stability of the particles (23).

The concentration of CNC aqueous suspension can affect the measured zeta-potential (26), too. So, the higher zeta-potential of CNC-II and CNC-III can be partly attributed to their higher concentration in comparison with CNC-I & IV (Fig. 1, Table 1).

Kandhola et al. (28) considered polydispersity index between 0.3 and 0.5 as a moderately homogeneous particle size distribution. The polydispersity index of more than 0.7 means that the suspension contains large particle agglomerates (13). The mean value of the polydispersity index was about 0.2-0.3 for all four suspensions (Table 1). It shows that the suspensions had rather good stability and consisted of uniform size distribution. Thus, the mean particle size achieved by DLS is reliable. However, the presence of agglomerates couldn't be ruled out completely just by the polydispersity index. Because there were several peaks in the size graphs based on intensity (Fig. S1). These peaks can be due to the rapid aggregation of nanocellulose suspended in water (19, 59), different size nano-particles, or a single particle rotating around different dimensions (45, 60, 61). The polydispersity index will be diminished with sonication energy (62). It is also likely that sonication energy or duration was not sufficient to break agglomerations. It is supposed that sonication at 60% amplitude for 10 minutes, can make only a moderately homogenous suspension of CNCs.

The surface charge density of CNCs originates from sulfate ester groups during sulfuric acid hydrolysis. It was also suggested that sulfur content may not be a good criterion of hydrolysis severity. The degree of sulfation and surface charge density can be determined with different methods, such as elemental analysis, zeta-potential (mV), and conductometric titration, which make it hard to make direct comparisons of data among studies. The degree of sulfation of CNCs is strongly dependent on hydrolysis circumstances, such as hydrolysis duration, acid concentration, acid-to-pulp ratio,

Table 2. The average zeta-potential, polydispersity index and mean diameter values of diluted CNC suspensions (0.025 wt%).

Sample	Zeta potential (mV)	Polydispersity Index	Diameter By Intensity (nm)	Diameter By Number (nm)	Diameter By Volume (nm)
CNC-I	− 24.58	0.4 ± 0.032	3878.19 ± 506.40	22.69 ± 0.96	386.70 ± 158.49
CNC-II	− 31.43	0.2 ± 0.024	306.15 ± 84.36	39.29 ± 16.34	136.67 ± 10.65
CNC-III	− 29.66	0.2 ± 0.021	129.10 ± 31.23	24.62 ± 14.48	32.17 ± 15.98
CNC-IV	− 26.96	0.3 ± 0.007	554.70 ± 143.27	144.44 ± 74.37	687.44 ± 288.21

and temperature (28). It seems that a higher acid-to-paper ratio could increase the degree of sulfation as CNC-III suspension had a higher zeta-potential. However, CNC-IV had a lower degree of sulfation based on zeta potential which shows the effect of acid-to-paper ratio is not permanent (Table 1). On the other hand, Kandhola et al. (28) did not observe a strong correlation between acid concentration, hydrolysis duration, and CNC sulfur content.

The increased particle size observed in CNC-I and CNC-IV is likely due to particle agglomerations, because the number-diameters and volume-diameters are somewhat lower than intensity-based diameters (Table 1). The concentrated acid (64 wt% H_2SO_4) was used during hydrolysis destroyed the majority of cellulose hydrogen bonding harshly, so the acid hydrolysis reaction was homogeneous and complete, which lead to a narrower nanocellulose size distribution (19) in CNC-III (Fig. 3) but not necessarily the higher surface charge, as CNC-IV has lower zeta-potential in comparison to CNC-III (Table 1). This result can prove that the concentration of acid is more effective than the volume of acid during hydrolysis reaction.

CNC-III had the highest zeta-potential and smallest size particles (Table 1). CNC-I & CNC-IV had apparent larger particles and weaker surface charge in comparison with CNC-II and CNC-III, which might be originated from nanocellulose inherent hydroxyl groups (19) (Table 1). CNC-I and CNC-IV had a relatively poor size dispersion based on size distribution graphs. Lower surface charge makes the suspension susceptible for aggregation and induces agglomerate of insoluble nanocellulose particles, resulting in wide-size dispersion (19) (Fig. 3, Table 1).

Longer hydrolysis duration and higher acid-to-pulp ratio have been shown to synthesize CNCs with shorter dimensions and narrower particle length distributions (63, 64). This claim can be rather true but not definite because CNC-III had shorter particles and a narrower distribution graph (Fig. 3) in comparison with CNC-II. However, CNC-IV had wider particle size distributions in comparison with the other suspensions (Fig. 3).

DLS-ELS: Diluted CNC suspensions (0.025 wt%)

The average intensity-diameters of CNC-II & III were lower than CNC-I & IV (Table 2). On the other hand, CNC-I had the largest diameter based on intensity (3878.19 ± 506.40 nm). This value can't be reliable mostly due to aggregation. The intensity-based graphs show several peaks for all four suspensions that mean the presence of agglomeration and clusters (Fig. S2). So, it was preferred to compare suspensions based on number distribution graphs (Fig. 4). Although the number-based graphs of CNC-I are superposed (Fig. 4), it can't rule out the presence of clusters (Fig. S2). Moreover, the polydispersity index of CNC-I was larger than three other samples that can show the presence of aggregations (Table 2). The number-based distribution patterns of diluted CNC-IV had also roughly two peaks for small size and large size particles (Fig. 4) that indicate the presence of clusters.

The zeta potentials obtained from diluted suspensions were in agreement with previous works (18, 65). It was mentioned before that dilution can affect DLS results and make them inaccurate. For all four suspensions, the obtained diameters are larger than the original suspensions (Table 1 & 2). This can be due to the fast aggregation of nanocellulose in water suspension (19). The presence of small aggregates has a rather large effect on DLS, too (27). It is reported that a strong surface charge prevents the nanocellulose particles from agglomeration (19). So, it seems that the zeta-potential in the range of 20-30 mV is not sufficient to prevent agglomerations in CNC suspensions, as the zeta-potential of CNC-I was - 24.58 mV, but the CNC diameter was overestimated mostly due to aggregations (Table 2).

On the other hand, the Brownian motion of negatively charged CNC particles is expected to be slowed down due to the presence of counterions in

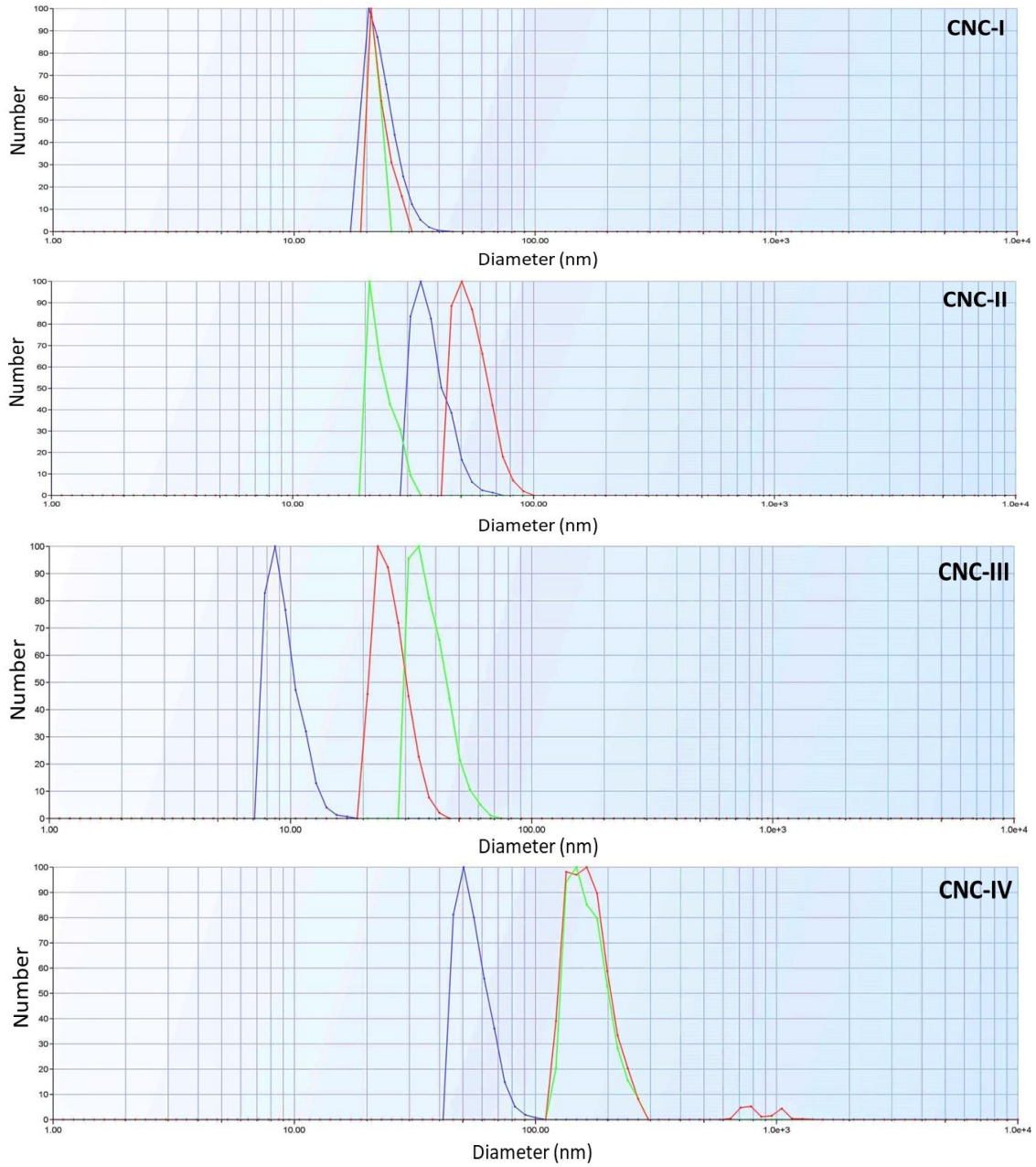

Fig. 4. The size distribution of diluted CNC suspensions (0.025 wt%) obtained from DLS. (Red: first run, Green: second run, Blue: third run)

the double layer, that called electroviscous effects (66, 67). This, as a result, decreases the translational diffusion coefficient and apparent particle size appears bigger than the real size (45). So it is assumed that the higher negative charge of diluted samples (especially CNC-I, III & IV) intensified the counterions in the double layer, so the translational diffusion decreased. As a result, the diameters of CNCs in diluted samples became larger than the original suspensions (Table 1 &2). Reid et al. (23) also reported that DLS measurements of less concentrated samples show multiple peaks and lead to inaccurate data due to the low scattering count, in contrast at higher concentrations, particle agglomeration will increase which causes larger apparent particle sizes. This claim can't be definite, either. Since the mean diameter of CNCs in the original suspensions was lower than diluted

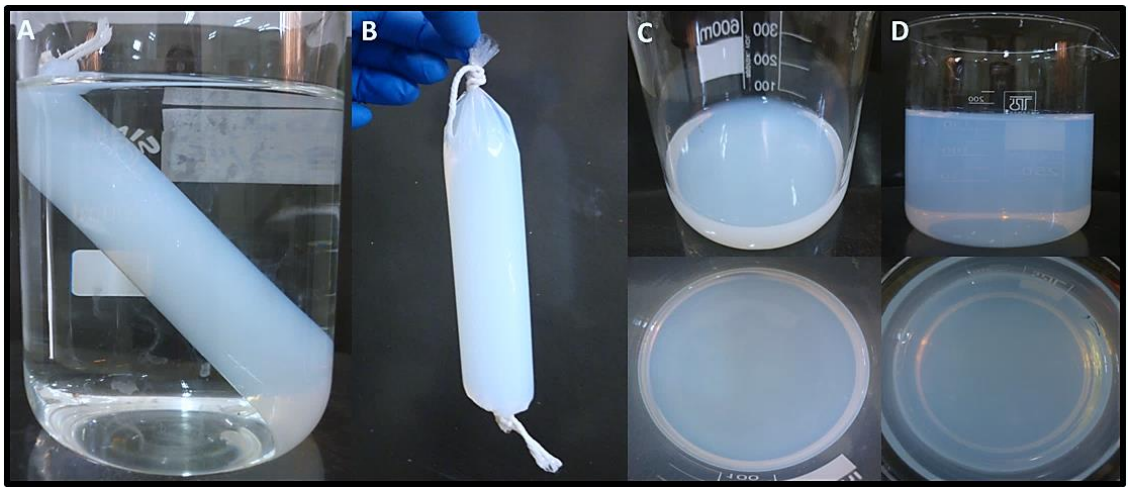

Fig. 5. A,B) The appearance of CNC-III suspension during dialysis, C) CNC-III suspension after evacuation from dialysis tube, D) CNC-III suspension after sonication and filtration.

samples in the present study (Table 1 & 2).

The CNC-II & CNC-III had higher absolute zeta-potentials in comparison with CNC-I and CNC-IV (Table 2) similar to previous results of original suspensions (Table 1). The CNC-III sample had the lowest diameters both in original and diluted suspensions (Table 1 & 2). It was also expected from the synthesis process that CNC-III would be a high-quality suspension because it had the best homogenous dispersion during the dialysis stage and a very nice light blue color (Fig. 5). There was sedimentation in dialysis tubes of CNC-I, CNC-II, and CNC-IV, but there was not any observable aggregation or precipitation in the dialysis tube of CNC-III. The DLS results confirmed the first prediction about the quality of CNC-III suspension.

Morphology of the CNCs by AFM:

A significant portion of particle behavior can be attributed to particle morphology (23). Figs. 6-9 display representative 5 × 5 µm & 10 × 10 µm AFM images of CNCs from each suspension. AFM images proved the presence of rod-shaped CNCs in all four suspensions. However, there were numerous aggregations in CNC-IV images that made it difficult to distinguish rod-shaped particles (Fig. 9A). The appearance of cellulose nanowhiskers was similar to previous studies (68, 69). Moreover, AFM images proved that the intensity-based diameters of CNC-I and CNC-IV obtained from DLS were not accurate and reliable. The length of two representative CNCs were shown in Fig. 10. It proves that DLS measurements of CNC-I and CNC-IV were absolutely overestimation.

The AFM images of CNC-II and CNC-III show that CNCs preserved their rod shape even after layering deposition (Fig. 7 & 8, C). Moreover, the annular pattern and chiral nematic structure of CNCs can be seen in Fig. 7C. The CNC-III suspension adopted a uniaxillary aligned nematic phase (Fig. 8C) like previous studies (33). But CNC-I & IV didn't have any special structure after layer by layer deposition (Figs. 6 & 9, C) and numerous agglomerations can be seen in Fig. 9C, too.

To summarize, all four suspensions contained nano dimension and rod-shaped cellulose crystalline (CNC) in this research that was confirmed by DLS and AFM results. Zhao et al. (51) reported that a lower acid-to-pulp ratio and the hydrolysis temperature result in CNCs with higher aspect ratios, which leads to the chiral nematic structure of CNCs. They found that the acid-to-pulp ratio is more effective than the hydrolysis temperature on the chiral nematic liquid crystal behavior. In contrast, the more harsh acid hydrolysis can ruin the lattice planes of cellulose, consequently disrupting the formation of the chiral nematic structure of CNC (51). The results of the present research signify this idea, too. AFM images of CNC-II and CNC-III showed annular and regular arrangements of CNCs (Figs. 7C & 8C) somewhat like chiral nematic patterns. In contrast, there wasn't any defined structure in AFM images of CNC-IV except some agglomerations (Fig. 9C) that can be due to higher acid-to-paper ratio and crystals cleavage.

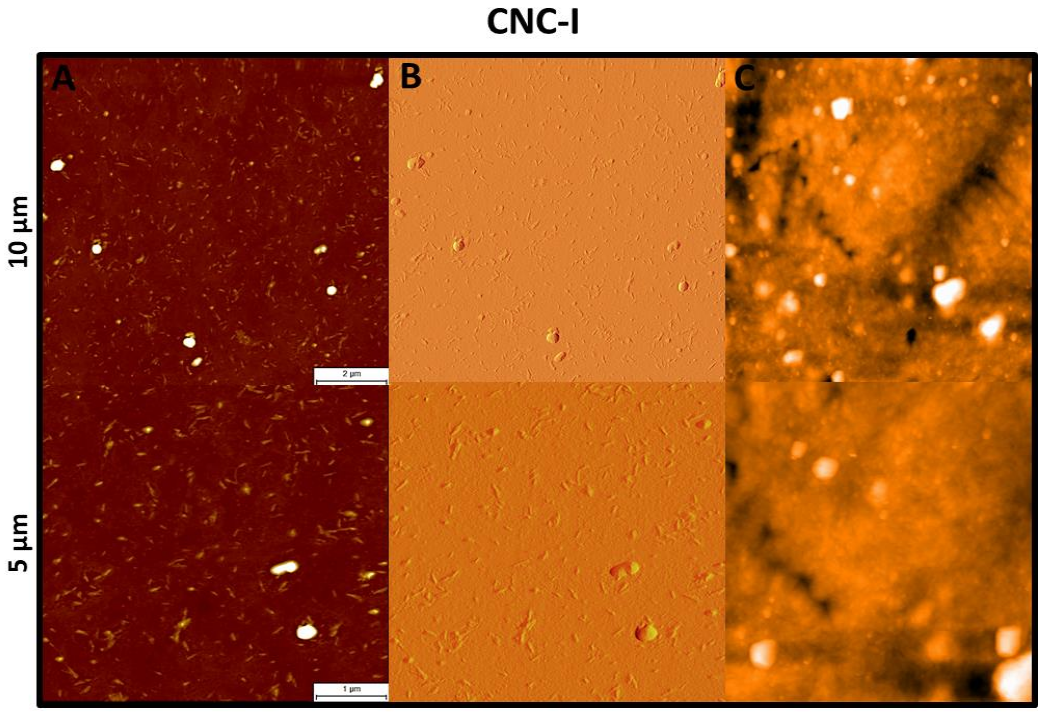

Fig. 6. AFM images of CNC-I suspension. A) Topography images of diluted CNCs (0.001 wt%) on silicon wafer with scan size of 10×10 µm and 5×5 µm, B) Correspondent amplitude images, C) Topography images of original suspension after layer by layer deposition

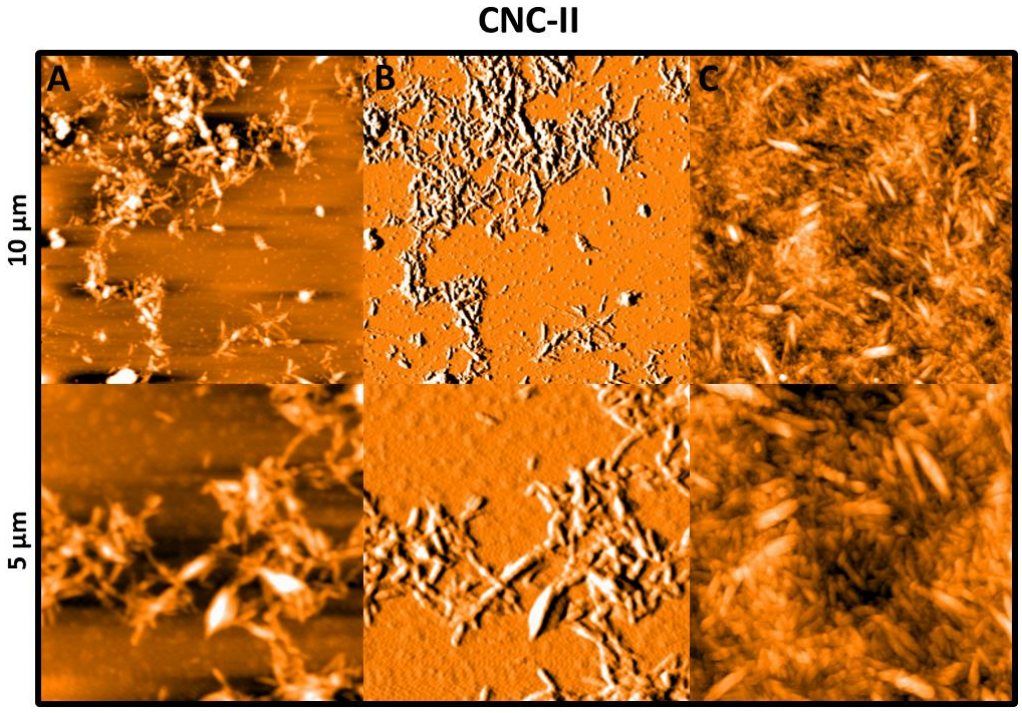

Fig. 7. AFM images of CNC-II suspension. A) Topography images of diluted CNCs (0.001 wt%) on glass substrate with scan size of 10×10 µm and 5×5 µm, B) Correspondent amplitude images, C) Topography images of original suspension after layer by layer deposition.

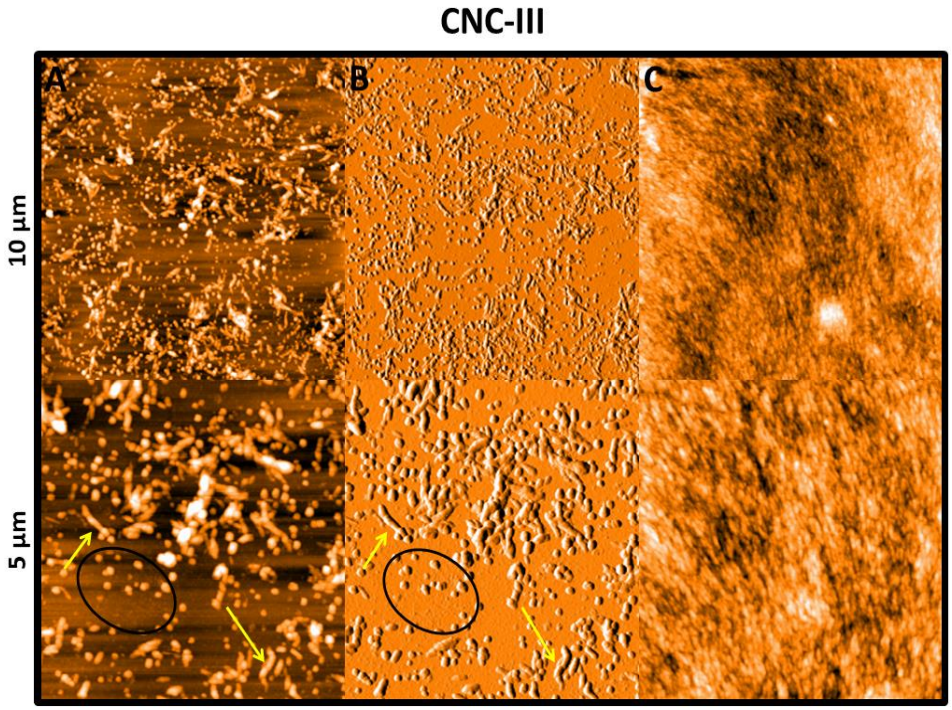

Fig. 8. AFM images of CNC-III suspension. A) Topography images of diluted CNCs (0.001 wt%) on glass substrate with scan size of 10×10 µm and 5×5 µm, B) Correspondent amplitude images, C) Topography images of original suspension after layer by layer deposition (The black ellipsoids show artifacts, and yellow arrows show CNCs with needle shape)

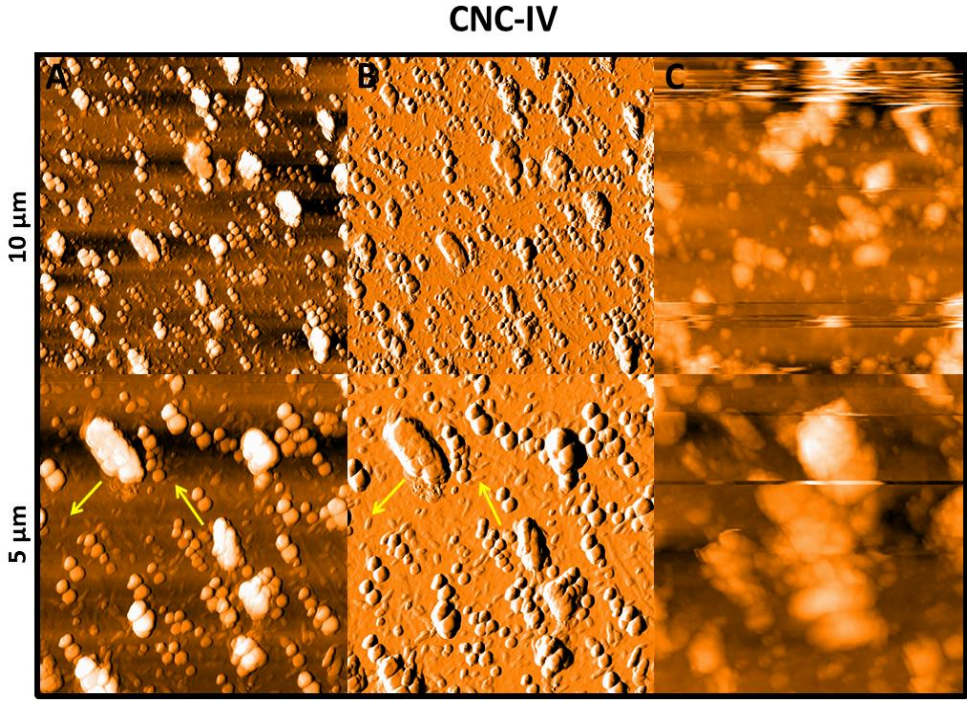

Fig. 9. AFM images of CNC-IV suspension. A) Topography images of diluted CNCs (0.001 wt%) on glass substrate with scan size of 10×10 µm and 5×5 µm, B) Correspondent amplitude images, C) Topography images of original suspension after layer by layer deposition. (The yellow arrows show CNCs with rod shape)

It is supposed that CNC-IV was over-hydrolyzed. The aggregates of over-hydrolyzed, degraded, re-precipitated cellulose, and large clumps were also observed, especially during the dialysis stage of the CNC-IV sample. There are also numerous micrometer size agglomerations in the AFM images of CNC-IV (Figs. 9A, B). It seems that the higher acid-to-paper ratio leads to shorter CNCs, due to more acid molecules available per unit mass of cellulose, on the contrary over hydrolization breaks nanocrystals and makes them susceptible for rapid agglomeration, too.

The AFM results of CNC-II and CNC-III prove that cellulose was uniformly dissolved with 64% sulfuric acid at 45 °C (Figs. 7C & 8C). The diameters and zeta potentials of CNC-II and CNC-III in diluted and original suspensions were consistent with each other, too. The intensity-based diameters of CNC-II and CNC-III had a minimum difference in original and diluted suspensions (Tables 1&2) which confirms the produced CNCs were homogenous at least in length.

It should be noted that CNCs are polar materials with surface charge and they will develop better interaction with a solvent that has a high solubility parameter through ion-dipole interactions (70, 71). The unsuitable solvents make CNCs undergo aggregation and cohesive particle-particle interactions (72). In the case of this study, double-distilled water was utilized in every phase of research. The diameter of CNCs increased after dilution in all four samples (Table 1 & 2). So, it is supposed that larger dimensions of CNCs after dilution can be somehow due to the application of double-distilled water that made the CNCs prone to aggregation. In contrast, there was not any significant change in the zeta-potentials after dilution (Table 1 & 2). It seems better to utilize deionized water for dilution of CNC suspensions to get more accurate and reliable results.

On the other hand, it is reported that particle sizes measured by DLS are not absolute and accurate (23, 48). Because DLS monitors the scattering intensity from particles undergoing Brownian motion and determines particle size via the Stokes-Einstein relation. This relation considers the diffusion coefficient constant but it is variable for rod-shaped particles such as CNCs. Since the diffusion constants perpendicular and parallel to the particle axis vary (23). The translational diffusion coefficient depends mainly on the particle length. Although the hydrodynamic diameter is not equal to actual particle length, it strongly correlates with particle length. The hydrodynamic radius of rods is much shorter than the actual particle length and does not have any physical meaning other than ranking rod-like particles of comparable diameters (45). Although DLS determines particle size based on a spherical model, if the sample is not aggregated, the particle size would be at least the size of the length (13). Boluk & Danumah (45) proposed to determine the length of CNCs by DLS and diameter (w) of CNCs by TEM or AFM. However, w (diameter) of CNCs would be overestimated due to the AFM tip broadening effect, and poor contrast of the particle edge in TEM images. There could be a complex relationship between the state of aggregation and surface charge which might affect either measurement (27).

Although both DLS and AFM can be utilized for CNC size measurements, there are a variety of limitations around the measurement of CNC by AFM. CNC aggregation is a big challenge during sample preparation for microscopy (Fig. 9A) and only single CNCs are measured. However, it is sometimes difficult to determine if a specific feature is due to one or several CNC particles. It is also difficult to completely standardize the AFM data analysis as different analysts may use slightly various criteria (27). It is necessary to prepare fractionated samples with low numbers of clusters to analyze CNCs more accurately via microscopy. On the other hand, the dispersion has a large effect in DLS measurements but not the AFM measurement, which is due to the presence of aggregates that are considered in the DLS results, but they are not analyzed by AFM (27). This is justified by the apparent large diameters of CNC-I and CNC-IV in the present research mostly due to aggregations that could not be distinguished from individual CNCs by DLS. The AFM results also proved that the real size of CNC-I and CNC-IV were much smaller (Fig. 10). In general, DLS results can be utilized for the comparison of relative sizes of cellulose nanocrystals (59). It provides statistical data to analyze the structures and dynamics of colloidal particles suspended or dispersed in a liquid (48). Besides, DLS is currently the fastest and cheapest method for CNC size characterization and would be beneficial for large-scale industrial applications (27).

It is important to optimize CNC synthesis and characterization techniques. Since CNC behavior and features affect its applications as rheological

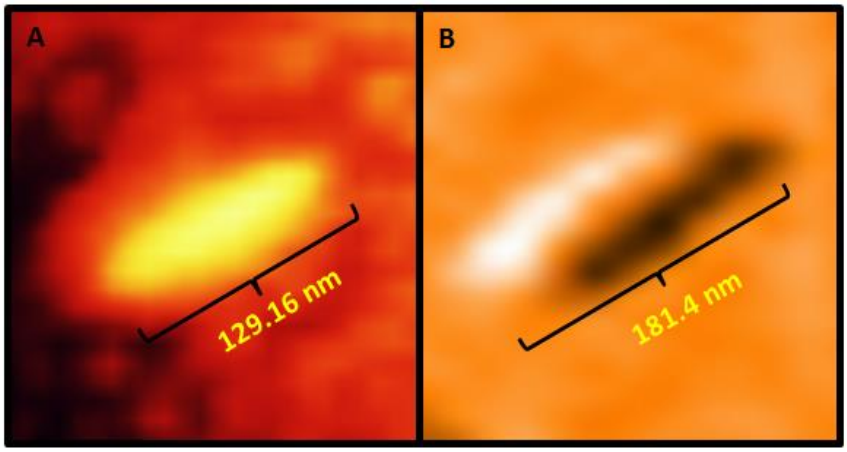

Fig. 10. The rod-shape and length of an individual CNC derived from AFM images (A: CNC-I, B: CNC-IV)

modifiers and reinforcing agents. The uniform dispersion of nanocellulose is important to improve the mechanical properties of nano-composite products (19). CNC behavior at an interface in nano-composites is not only dependent on surface charge density but also the aspect ratio of particles. Particles with higher aspect ratios, form gels and percolated networks at lower concentrations, so the amount of material needed for specific applications will be reduced. It has been shown that the higher charge density in environments with elevated ionic strengths has a significant effect on particles behavior at interfaces (23).

Beck-Candanedo et al. (73) reported that a higher acid-to-pulp ratio decreases nanocrystal dimensions to some extent at the reaction time of 45 min. At the shorter reaction time of 25 min, the effect of the acid-to-pulp ratio on critical concentration and rod dimensions may be more apparent (73). In the present study, as the acid-to-paper ratio was increased, there was a decrease in the diameters of CNCs. This reduction of diameters was also significant from 20:1 mL/g to 30:1 mL/g. However, increasing the acid-to-paper ratio from 30 mL/g to 40 mL/g didn't have a well-defined influence on the particle size reduction, in contrast, made the suspension prone to agglomerations (Table 1&2, Fig. 9).

Feng et al. (29) reported that the hydrolysis mixture became a yellow slurry after 45 min vigorous stirring to produce CNCs, but it was concluded from the present research that there is not any necessity for obtaining yellow slurry to be sure about CNC production. As it is seen in Fig. 2, CNC-II and CNC-III hydrolysis mixtures are not yellow at all. In contrast, they are white and somewhat creamy, respectively. The hydrolysis mixture doesn't have to be slurry, either. It seems that a hydrolysis mixture in the form of cream or porridge is more suitable for CNC production. On the other hand, vigorous stirring is not appropriate for CNC synthesis as Yang (16) also utilized a low stirring rate for CNC production.

Beck-Candanedo et al. (73) reported that larger volumes of the 64 wt % acid can hydrolyze a given amount of pulp faster and produce shorter rods for a given reaction time, but the effect is not considerable. They found that the acid-to-pulp ratio did not have a well-defined effect on the sulfur content of the wood cellulose suspensions. They observed shorter rods and the lower total surface charge by a higher acid-to-pulp ratio (73).

DLS results of CNC-I, CNC-II, and CNC-III in the present research showed that a higher acid-to-paper ratio can lead to smaller size CNCs (Table 1 & 2). This finding is almost consistent with Beck-Candanedo's (73) observations. However, the effect of a higher acid-to-paper ratio was not significant for CNC-IV. In fact, all three kinds of diameters (intensity, number, volume) obtained by DLS should be considered for an accurate conclusion about CNC size. In this regard, the higher acid-to-paper ratio had tended to reduce particle size even in CNC-IV suspension (Table 1 & 2, Fig. 10), but this effect was not significant as Beck-Candanedo's (73) claim. The acid-to-paper ratio did not have a well-defined effect on the polydispersity index in this research (Table 1 & 2), too. Moreover, a higher acid-to-paper ratio does not necessarily increase the surface charge of CNCs. As the acid-to-paper

ratio was increased from 10:1 mL/g to 30:1 mL/g the surface charge also increased, but it decreased again after increasing the acid-to-paper ratio from 30:1 mL/g to 40:1 mL/g (Table 1 & 2). This is consistent with Beck-Candanedo et al.'s (73) study. Brito et al. (74) also hydrolyzed Bamboo fibers with 65 wt% sulfuric acid at an acid/fiber ratio of 10:1 mL/g and 15:1 mL/g at 60 °C for 12 minutes. As acid/fiber was increased, the zeta-potential changed from -59±2 mV to -54±1 mV which shows the negative surface charge decreased. A similar result was obtained in this research, too. The negative surface charge of CNC-IV was lower than CNC-III in both original and diluted samples (Table 1&2).

In the end, it should be mentioned that no single characterization technique can determine particle behavior and properties precisely (23). Since aggregation of particles causes an overestimation of particle diameter using DLS, further analysis like AFM will be helpful to determine CNC diameter more accurately (17). However, DLS measures the whole suspension at once, while the sample set of particles used for size measurement in AFM is small and may not be representative of the bulk sample (27). Sonication may increase the number of larger individual particles available for AFM analysis because it disperses the agglomerates (62). So, AFM study of CNCs after sonication may result in higher size CNCs in comparison with DLS; this is exactly what was observed in Brinkmann et al.'s (62) study. They suggested that disrupting agglomerates by sonication changes the fraction of longer particles (62). DLS is good for inter batch comparisons particularly when the PDI of the sample is low, but DLS results cannot be directly correlated to the AFM results, because AFM enables the direct measurement of the particle length and height (27). Moreover, DLS provides an equivalent hydrodynamic diameter and intensity weighted distribution whereas microscopy gives a number weighted distribution. DLS provides insight into the dispersion of nanoparticles in suspension, while the size measurement of AFM is a physical size but a two-dimensional projection of a three-dimensional system (41, 62). So, it would be difficult to compare DLS and AFM results directly.

Despite the charged surfaces which lead to colloidal stable suspensions, CNCs have a high tendency to aggregate in suspension and when deposited on a substrate. This is an important limitation for microscopy since agglomerated particles must be excluded from the analysis. Sampling is a very challenging and time-consuming procedure for microscopic analysis of CNCs. The selection of individual CNCs for analysis is subjective, and the analyst decides which particles can be counted from microscopy results (62). On the other hand, the applicability of DLS for rod-shaped nanomaterials and comparing intensity-to-number-based distributions are the other challenges of CNC analysis. So both DLS and AFM techniques must be standardized for attaining the most reliable results about CNC dimensions.

CONCLUSIONS:

Cellulose nanocrystals (CNCs) were successfully extracted from Whatman #1 filter paper by acid hydrolysis. CNC suspensions were moderately stable electrostatically and showed rod-like shapes. The treatment of Whatman #1 filter paper with 64 wt% sulfuric acid at an acid-to-paper ratio of 20:1 mL/g & 30:1 mL/g at 45°C (60 min) is appropriate for CNC synthesis because CNCs had smaller size and more surface negative charge. Furthermore, the helical structures and regular orientation of CNCs were observed in AFM images. However, a higher acid-to-paper ratio does not necessarily produce smaller CNCs with higher zeta-potential, because the CNC-IV sample that was produced at an acid/paper ratio of 40:1 mL/g had larger particles and lower zeta-potential. It is also found that white or creamy hydrolysis mixture results in homogenous CNCs with lower size, higher zeta-potential, and better self-organization. On the other hand, yellow or brown hydrolysis mixture decreases the quality of CNCs and it is a sign of damage to the crystals. The polydispersity index of CNC suspensions is better to be lower than 0.2 to get the most accurate and reliable dimension by DLS and make a reasonable comparison between CNC suspensions. The zeta-potential lower than -30 mV is suitable for CNC suspensions as a more negative surface charge enhances the stability of the suspension. The blue color of the final CNC aqueous suspension can be a kind of criteria for distinguishing high-quality CNCs. Moreover, all three kinds of diameters via DLS (intensity-number-volume) should be considered for a better understanding of CNC subpopulations. It seems that a gentle and constant stirring rate is more appropriate for CNC production on a lab scale rather than vigorous stirring. It is also worth examining the stirring rate as an independent parameter for CNC synthesis in future studies. All beginners in the CNC field

may benefit from the procedures and results of this work.

SUPPORTING INFORMATION:

Size distribution of original CNC suspensions by intensity (Fig. S1), the size distribution of diluted CNC suspensions (0.025 wt%) by intensity (Fig. S2)

CONFLICT OF INTEREST:

The authors declare that there is no conflict of interest regarding the publication of this manuscript.

REFERENCES

1. S A. Cellulose/calcium phosphate hybrids: New materials for biomedical and environmental applications. International Journal of Biological Macromolecules. 2019.
2. SS GJ. Cellulose nanocrystals: synthesis, functional properties, and applications. Nanotechnology, Science and Applications. 2015;8:45-54. https://doi.org/10.2147/NSA.S64386
3. Lizundia E PD NT-D, Armentano I. Cellulose nanocrystal based multifunctional nanohybrids. Progress in Materials Science. 2020. https://doi.org/10.1016/j.pmatsci.2020.100668
4. Yang Y CZ ZJ, Wang G, Zhang R, Dingjie S. Preparation and Applications of the Cellulose Nanocrystal. International Journal of Polymer Science. 2019. https://doi.org/10.1155/2019/1767028
5. A S. An investigation of carbon nanotubes on shear stress, thermal conductivity and the viscosity of Nanofluids. Journal of Nanoanalysis. 2020;7(4):1-7.
6. A S. Using NiFe 2 O 4 as a nano photocatalyst for degradation of polyvinyl alcohol in synthetic wastewater. Environmental Challenges. 2021;5. https://doi.org/10.1016/j.envc.2021.100332
7. Karimi S SA. The removal of Hexavalent chromium; (Cr (VI)) by ZnO/LECA as a nano photocatalyst using full factorial experimental design. Journal of Nanoanalysis. 2021;8(3):167-75.
8. A S. Employing Sono-Fenton Process for Degradation of 2-Nitrophenol in Aqueous Environment Using Box-Behnken Design Method and Kinetic Study1. Russian Journal of Physical Chemistry A. 2019;93(2):243-49. https://doi.org/10.1134/S003602441902002X
9. A S. Using Mn based on lightweight expanded clay aggregate (LECA) as an original catalyst for the removal of NO2 pollutant in aqueous environment. Surfaces and Interfaces. 2020;21. https://doi.org/10.1016/j.surfin.2020.100705
10. Saghi M SA, Arastehnodeh A, Khazaeinejad M, Nozari A. The photo degradation of methyl red in aqueous solutions by α-Fe2O3/SiO2 nano photocatalyst. Journal of Nanoanalysis. 2018;5(3):163-70.
11. Hekmatshoar R YA, Shokri A. Using ZnO based on Bentonite as a nano photocatalyst for degradation of Acid Red 114 in synthetic wastewater. Journal of Nanoanalysis. 2020;7(4):1-10.
12. A S. Degradation of Terphetalic Acid from Petrochemical Wastewater by Ozonation and O3/ZnO Processes in Semi Batch Reactor. Archives of Hygiene Sciences. 2017;6(4):348-55. https://doi.org/10.29252/ArchHygSci.6.4.348
13. Albernaz VL JG LC, Silva LP. Cellulose Nanocrystals Obtained from Rice By-Products and Their Binding Potential to Metallic Ions. Journal of Nanomaterials. 2015. https://doi.org/10.1155/2015/357384
14. Elfeky AS SS EA, Owda ME, Eladawy HA, Saeed AM, Awad MA, Abou-Zeid RE, Fouda A. Multifunctional cellulose nanocrystal /metal oxide hybrid, photo-degradation, antibacterial and larvicidal activities. Carbohydrate Polymers. 2019. https://doi.org/10.1016/j.carbpol.2019.115711
15. Kargarzadeh H IM AI, Thomas S, Dufresne A. Handbook of Nanocellulose and Cellulose Nanocomposites. KGaA: Wiley-VCH Verlag GmbH & Co; 2017. https://doi.org/10.1002/9783527689972
16. Y J. MANUFACTURING OF NANOCRYSTALLINE CELLULOSE. Espoo, Finland: Aalto University; 2017.
17. N C. Preparation and characterization of nanocellulose from wheat bran: Lund University; 2017.
18. Nascimentoa JHOD LR GF, Melob JDD, Oliveiraa FR, Ladchumananandasivama R, Zillec A. Extraction and Characterization of Cellulosic Nanowhisker obtained from Discarded Cotton Fibers. Materials Today: Proceedings. 2015;2:1-7. https://doi.org/10.1016/j.matpr.2015.04.001
19. Zhou YM FS ZL, Zhan HY. Effect of nanocellulose isolation techniques on the formation of reinforced poly(vinyl alcohol) nanocomposite films. eXPRESS Polymer Letters. 2012;6(10):794-804. https://doi.org/10.3144/expresspolymlett.2012.85
20. Maturavongsadit P PG SR, Benhabbour SR. Thermo-/pH-Responsive Chitosan-Cellulose Nanocrystal Based Hydrogel with Tunable Mechanical Properties for Tissue Regeneration Applications. Materialia. 2020;12. https://doi.org/10.1016/j.mtla.2020.100681
21. HY LP. Preparation and properties of cellulose nanocrystal: Rods, spheres, and network. Carbohydrate Polymers. 2010;82:329-36. https://doi.org/10.1016/j.carbpol.2010.04.073
22. Ferla BL ZL BP, Gennaro PD. Cellulose nanocrystals as promising nanodevices in the biomedical field. AIP Conference Proceedings. 2018. https://doi.org/10.1063/1.5047773
23. Reid MS VM CE. Benchmarking Cellulose Nanocrystals: From the Laboratory to Industrial Production. Langmuir. 2017;33(7):1583-98. https://doi.org/10.1021/acs.langmuir.6b03765
24. Prathapan R TR GG, Hu J. The recent progress of cellulose nanocrystals alignment and its applications. ACS Applied Biomaterials. 2020. https://doi.org/10.1021/acsabm.0c00104
25. E D. Basic Principles of Colloid Science. Cambridge: The Royal Society of Chemistry; 1988.
26. Rehman N BC MM, Rosa SML. Dynamics of Cellulose Nanocrystals in the Presence of Hexadecyltrimethylammonium Bromide. Macromolecular Research. 2017. https://doi.org/10.1007/s13233-017-5089-6
27. L T. Cellulose Nanocrystals: Particle Size Distribution and Dispersion in Polymer Composites. Ottawa, Canada: University of Ottawa; 2016.
28. Kandhola G DA RK, Labbé N, Sakon J, Carrier DJ, Kim JW. Maximizing production of cellulose nanocrystals and nanofibers from pre-extracted loblolly pine kraft pulp: a response surface approach. Bioresources and Bioprocessing.

2020;7(19). https://doi.org/10.1186/s40643-020-00302-0
29. Feng. Improving homogeneity of iridescent cellulose nanocrystal films by surfactant assisted spreading self-assembly. ACS Sustainable Chemistry & Engineering. 2019;7(23):19062-71. https://doi.org/10.1021/acssuschemeng.9b04875
30. Hamad. 2017.
31. Santana MF SM YF, Moreira BC, Almeida JMD, Teixeira AVNDC, Silva DDJ. CELLULOSE NANOCRYSTAL PRODUCTION FOCUSING ON CELLULOSIC MATERIAL PRE-TREATMENT AND ACID HYDROLYSIS TIME. O PAPEL. 2019;80(03):59-66.
32. MascheroniE RR OM, Piva G, Bonetti S, Piergiovanni L. Comparison of cellulose nanocrystals obtained by sulfuric acid hydrolysis and ammonium persulfate, to be used as coating on flexible food-packaging materials. Cellulose. 2016. https://doi.org/10.1007/s10570-015-0853-2
33. MX GD. Chiral nematic structure of cellulose nanocrystal suspensions and films; Polarized light and atomic force microscopy. Materials. 2015;8(11):7873-88. https://doi.org/10.3390/ma8115427
34. H W. Cellulose nanocrystals: properties, production, and applications. Chichester: John Wiley & Sons; 2017.
35. Hynninen V MP WW, Hietala S, Linder MB, Ikkala O, Nonappa. Methyl cellulose/cellulose nanocrystal nanocomposite fibers with high ductility. European Polymer Journal. 2019;112:34-45. https://doi.org/10.1016/j.eurpolymj.2018.12.035
36. Ivanova A F-PB PA, Wagner T, Jumabekov AN, Vilk Y, Weber J, Gunne J, Vignolini S, Tiemann M, Fattakhova-Rohlfing D, Bein T. Cellulose nanocrystal-templated tin dioxide thin film for gas sensing. ACS Applied Materials & Interfaces. 2020;12(11):12639-47. https://doi.org/10.1021/acsami.9b11891
37. Li W JB ZS. Preparation of cysteamine-modified cellulose nanocrystal adsorbent for removal of mercury ions from aqueous solutions. Cellulose. 2019;26:4971-85. https://doi.org/10.1007/s10570-019-02420-1
38. Or T SS EA, Osorio DA, De France KJ, Vapaavuori J, Hoare T, Cerf A, Cranston ED, Moran-Mirabal JM. Patterned cellulose nanocrystal aerogel films with tunable dimensions and morphologies as ultra-porous scaffolds for cell culture. ACS Applied Nano Materials. 2019;2(7):4169-79. https://doi.org/10.1021/acsanm.9b00640
39. Wang J PT XZ, Nigmatullin R, Harniman RL, Eichhorn SJ. Cellulose nanocrystal-polyetherimide hybrid nanofibrous interleaves for enhanced interlaminar fracture toughness of carbon fibre/epoxy composites. Composites Science and Technology. 2019;182. https://doi.org/10.1016/j.compscitech.2019.107744
40. Zhao TH PR WC, Lim KTP, Frka-Petesic B, Vignolini S. Printing of responsive photonic cellulose nanocrystal microfilm arrays. Advanced Functional Materials. 2019;29(21). https://doi.org/10.1002/adfm.201804531
41. Vanderfleet OM OD CE. Optimization of cellulose nanocrystal length and surface charge density through phosphoric acid hydrolysis. Philosiphical Transactions A royalsocietypublishing. 2017;376. https://doi.org/10.1098/rsta.2017.0041
42. Kano FS SA RD. Variation of the milling conditions in the obtaining of nanocellulose from the paper sludge. RevistaMateria. 2019;24(3). https://doi.org/10.1590/s1517-707620190003.0719
43. Jakubek ZJ CM CM, Leng T, Liu L, Zou S, Baxa U, Clogston JD, Hamad WY, Johnston LJ. Characterization challenges for a cellulose nanocrystal reference material: dispersion and particle size distributions. Journal of Nanoparticle Research. 2018;20. https://doi.org/10.1007/s11051-018-4194-6
44. Sadeghifar H FI, Clarke SP, Brougham DF, Argyropoulos DS. Production of cellulose nanocrystals using hydrobromic acid and click reactions on their surface. Journal of Materials Science. 2011;46:7344-55. https://doi.org/10.1007/s10853-011-5696-0
45. DC BY. Analysis of Cellulose Nanocrystal Rod Lengths by Dynamic Light Scattering and Electron Microscopy. Journal of Nanoparticle Research. 2014;16(1):2174. https://doi.org/10.1007/s11051-013-2174-4
46. Chen M PJ MA, Couillard M, Zou S, Hackley VA, Johnston LJ. Characterization of size and aggregation for cellulose nanocrystal dispersions separated by asymmetrical-flow field-flow fractionation. Cellulose (Lond). 2019;27(4). https://doi.org/10.1007/s10570-019-02909-9
47. Scognamiglio F SC RG. Extraction of Cellulose Nanocrystals (NCC) from Cotton Waste and Morphology of NCC Obtained with Different Alkali Neutralization. Current Journal of Applied Science and Technology. 2019;36(5):1-8. https://doi.org/10.9734/cjast/2019/v36i530254
48. Zhou Y FS ST, Isogai A. Characterization of Concentration-Dependent Gelation Behavior of Aqueous TEMPO-Cellulose Nanocrystal Dispersions Using Dynamic Light Scattering. Biomacromolecules. 2018.
49. Balding P LM WQ, Volkovinsky R, Russo P. Cellulose Nanocrystal–Polyelectrolyte Hybrids for Bentonite Water-Based Drilling Fluids. ACS Applied Biomaterials. 2020. https://doi.org/10.1021/acsabm.0c00071
50. AY PV. Nanosuspension: an approach to enhance solubility of drugs. J Adv Pharm Technol Res. 2011;2:81-7. https://doi.org/10.4103/2231-4040.82950
51. Zhao G ZS ZS, Pan M. Fabrication and characterization of photonic cellulose nanocrystal films with structural colors covering full visible light. Journal of Material Science, Polymers & biopolymers. 2020. https://doi.org/10.1007/s10853-020-04616-4
52. Qiao C CG ZJ, Yao, J. Structure and rheological properties of cellulose nanocrystals suspension. Food Hydrocolloids. 2016;55:19-25. https://doi.org/10.1016/j.foodhyd.2015.11.005
53. Leite LSF FC CeA, Moreira FKV, Mattoso LHC. Scaled-up production of gelatin-cellulose nanocrystal bionanocomposite films by continuous casting. Carbohydrate Polymers. 2020. https://doi.org/10.1016/j.carbpol.2020.116198
54. Han JQ ZC WY, Liu FY, Wu QL. Selfassembling behavior of cellulose nanoparticles during freeze-drying: effect of suspension concentration, particle size, crystal structure, and surface charge. Biomacromolecules. 2013;14:1529-40. https://doi.org/10.1021/bm4001734
55. Mabrouk AB DA BS. Cellulose nanocrystal as ecofriendly stabilizer for emulsion polymerization and its application for waterborne adhesive. Carbohydrate Polymers. 2019. https://doi.org/10.1016/j.carbpol.2019.115504
56. B Z. Multi-functional coating of polymeric spherulites for chiral photonic cellulose nanocrystal films. Cellulose. 2020.
57. Samadder R AN RA, Uddin M, Hossen J, Azam S. Magnetic nanocomposite based on polyacrylic acid and carboxylated

cellulose nanocrystal for the removal of cationic dye. RSC Advances. 2020;10:11945-56. https://doi.org/10.1039/D0RA00604A
58. Jia C CL SZ, Agarwal UP, Hu L, Zhu JY. Using a fully recyclable dicarboxylic acid for producing dispersible and thermally stable cellulose nanomaterials from different cellulosic sources. Cellulose. 2017;24(6):2483-98. https://doi.org/10.1007/s10570-017-1277-y
59. Ribeiro RSA BN JN. Statistical analysis of the crystallinity index of nanocellulose produced from Kraft pulp via controlled enzymatic hydrolysis. Biotechnology and Applied Biochemistry. 2019. https://doi.org/10.1002/bab.1873
60. Shanmugarajah B KP CI, Choong TSY, Tan KW. Isolation of nanocrystalline cellulose (NCC) from palm oil empty fruit bunch (EFB): Preliminary result on FTIR and DLS analysis. Chemical Engineering Transactions. 2015;45:1705-10.
61. Rashtchian M HA BS, Milan PB, Simorgh S. Fabricating alginate/poly(caprolactone) nanofibers with enhanced bio-mechanical properties via cellulose nanocrystal incorporation. Carbohydrate Polymers. 2020. https://doi.org/10.1016/j.carbpol.2020.115873
62. Brinkmann A CM CM, Jakubek ZJ, Leng T, Johnston LJ. Correlating Cellulose Nanocrystal Particle Size and Surface Area. Langmuir. 2016;32:6105−14. https://doi.org/10.1021/acs.langmuir.6b01376
63. Sun B ZM HQ, Liu R, Wu T, Si C. Further characterization of cellulose nanocrystal (CNC) preparation from sulfuric acid hydrolysis of cotton fibers. Cellulose. 2016;23:439-50. https://doi.org/10.1007/s10570-015-0803-z
64. Ren S SX LT, Wu Q. The effect of chemical and high-pressure homogenization treatment conditions on the morphology of cellulose nanoparticles. J Nanomater. 2014. https://doi.org/10.1155/2014/582913
65. Pinheiro JA MN, Villetti MA, Balaban RDC. Polymer-Decorated Cellulose Nanocrystals as Environmentally Friendly Additives for Olefin-Based Drilling Fluids. International Journal of Molecular Sciences. 2021;22(352). https://doi.org/10.3390/ijms22010352
66. Boluk Y LR ZL, McDermott MT. Suspension viscosities and shape parameter of cellulose nanocrystals (CNC). Colloids Surf A. 2011;377(1-3):297-303. https://doi.org/10.1016/j.colsurfa.2011.01.003
67. PA WA. Low-shear viscosities of (semi-)dilute, aqueous dispersions of charged boehmite rods: dynamic scaling of double layer effects. Langmuir. 1997;13(17):4574-82. https://doi.org/10.1021/la9700477
68. Kuang Y LX, Luan P, Zhang X, Xu J, Mo L, Gong J, Li J. Cellulose II nanocrystal: a promising bio-template for porous or hollow nano SiO2 fabrication. Cellulose. 2020. https://doi.org/10.1007/s10570-020-02973-6
69. Diao H ZZ, Liu Y, Song Z, Zhou L, Duan Y, Zhang J. Facile fabrication of carboxylated cellulose nanocrystal-MnO2 beads for high-efficiency removal of methylene blue. Cellulose. 2020. https://doi.org/10.1007/s10570-020-03260-0
70. Prihatiningtyas I LY HY, Vananroye A, Coenen N, Van der Bruggen B. Effect of solvent on the morphology and performance of cellulose triacetate membrane/cellulose nanocrystal nanocomposite pervaporation desalination membranes. Chemical Engineering Journal. 2020.
71. Lagerwall JPF StC SM, Noh JH, Park JH, Scalia G, Bergstro¨m L. Cellulose nanocrystal-based materials: From liquid crystal self-assembly and glass formation to multifunctional thin films. NPG Asia MateriaL. 2014;1(6):1-12. https://doi.org/10.1038/am.2013.69
72. Reid MS VM CE. Cellulose Nanocrystal Interactions Probed by Thin Film Swelling to Predict Dispersibility. Nanoscale. 2016;8(24):12247-57. https://doi.org/10.1039/C6NR01737A
73. Beck-Candanedo S RM GD. Effect of Reaction Conditions on the Properties and Behavior of Wood Cellulose Nanocrystal Suspensions. Biomacromolecules. 2005;6(2):1048-54. https://doi.org/10.1021/bm049300p
74. Brito BSL PF PJ, Jean B. Preparation, morphology and structure of cellulose nanocrystals from babmboo fibers. Cellulose. 2012;19:1527-36. https://doi.org/10.1007/s10570-012-9738-9